Original Research Article | Open Access

The Journal of Cardiovascular Aging

Xu et al. J Cardiovasc Aging. 2026;6:35 DOI:10.20517/jca.2026.14

CARD10 deficiency attenuates myocardial infarction associated with enhanced cardiac fibroblast senescence

Yueyue Xu[1,2,#], Yiwei Yao[1,#], Yueyun Zhou[1,#], Ganyi Chen[1], Yafeng Liu[1], Yunfei Jiang[1,3], Xu Cao[1], Wanlin Li[1], Yide Cao[1], Wen Chen[1], Xin Chen[1]

Keywords:
Myocardial infarction, senescence, mitochondria, aging

Citation: Xu Y, Yao Y, Zhou Y, Chen G, Liu Y, Jiang Y, Cao X, Li W, Cao Y, Chen W, Chen X. CARD10 deficiency attenuates myocardial infarction associated with enhanced cardiac fibroblast senescence. *J Cardiovasc Aging.* 2026;6:35. https://dx.doi.org/10.20517/jca.2026.14

Received: 4 Feb 2026
First Decision: 1 Jun 2026
Revised: 24 Jun 2026
Accepted: 4 Aug 2026
Published: 28 Aug 2026

Academic Editor:
Houzao Chen
Copy Editor:
Ping Zhang
Production Editor:
Ping Zhang

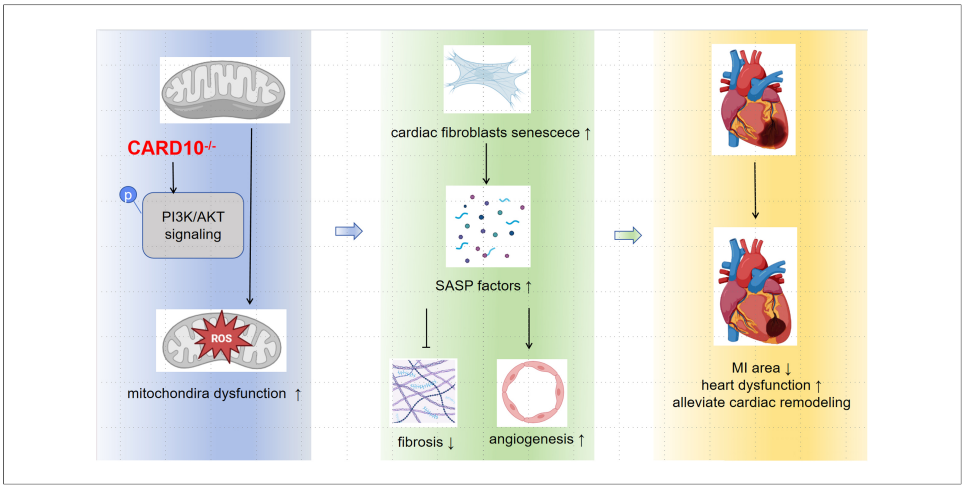

Abstract

Aim: Myocardial infarction (MI) causes cardiomyocyte death and triggers tissue repair and remodeling processes orchestrated by multiple cell types, particularly cardiac fibroblasts (CFs). Caspase recruitment domain-containing protein 10 (CARD10) has been implicated in mitochondrial function and aneurysm formation; however, its role in MI is not clear. To investigate the potential role of CARD10 in MI and the underlying mechanisms.

Methods: CARD10 expression and localization were analyzed by Western blot and immunofluorescence in mouse and human heart tissues. CARD10-deficient (*Card10*$^{-/-}$) and wild-type (WT) mice were subjected to experimental MI. Cardiac structure and function were assessed by echocardiography, histological analysis, and triphenyltetrazolium chloride (TTC). Cellular senescence was evaluated *in vivo* and in primary CFs using senescence-associated β-galactosidase (SA-β-gal) staining and the expression of p16 and phosphorylated histone H2A.X (gH2A.X). Mitochondrial dysfunction was assessed by JC-1

[1]Department of Thoracic and Cardiovascular Surgery, Nanjing First Hospital, Nanjing Medical University, Nanjing 210006, Jiangsu, China.
[2]INSERM UMR1180, University of Paris-Saclay, Orsay 91190, France.
[3]Department of cardiac surgery, Nanjing Drum Tower Hospital, Nanjing 210008, Jiangsu, China.
[#]These authors contributed equally to this work.

Correspondence to: Prof. Xin Chen, Dr. Wen Chen, Department of Thoracic and Cardiovascular Surgery, Nanjing First Hospital, Nanjing Medical University, Nanjing 210006, Jiangsu, China. E-mail: stevecx@njmu.edu.cn; cxacf@163.com

staining, mitochondrial reactive oxidative species (mtROS) measurements, and transmission electron microscopy. Potential signaling pathways were investigated by Western blot analysis.

Results: Following MI, CARD10 expression was increased in the infarct border zone and was predominantly localized with CFs. *Card10*$^{-/-}$ attenuated myocardial injury, improved cardiac remodeling, and enhanced fibroblast senescence. In vitro, transforming growth factor-beta (TGF-β)-stimulated *Card10*$^{-/-}$ CFs exhibited increased senescence, accompanied by elevated secretion of senescence-associated secretory phenotype (SASP) factors. Conditioned media from *Card10*$^{-/-}$ CFs promoted endothelial cell proliferation and angiogenesis. Furthermore, *Card10*$^{-/-}$ CFs exhibited severe mitochondrial dysfunction and activation of the phosphoinositide 3-kinase (PI3K) /protein kinase B (AKT) signaling pathway.

Conclusion: These findings suggest that CARD10 deficiency is associated with enhanced fibroblast senescence and improved post-MI remodeling, potentially involving mitochondrial dysfunction and PI3K/AKT signaling, highlighting CARD10 may represent a promising target for the treatment of MI.

INTRODUCTION

With increasing life expectancy and improvements in living standards, the global incidence of cardiovascular diseases continues to rise[1], imposing a heavy burden on healthcare systems. This burden is particularly pronounced among older adults, males, and populations in rural areas, where both mortality and economic impact are significantly elevated[2]. Among cardiovascular diseases, myocardial infarction (MI) represents a significant global health burden due to its high rates of morbidity and mortality[3]. Despite advances in clinical management, improving outcomes following MI remains a major research priority.

MI results in extensive cardiomyocyte death. Due to the negligible regenerative capacity of adult cardiomyocytes, other cells, particularly cardiac fibroblasts (CFs), play a central role in orchestrating scar formation post-infarction[4]. Following ischemic injury, activated CFs replace necrotic tissue, produce an extracellular matrix (ECM) scaffold, and modulate inflammatory and angiogenic responses through secretion of a variety of cytokines such as interleukin-6 (IL-6), transforming growth factor-beta (TGF-β), interleukin-1beta (IL-1β), and platelet-derived growth factor AA (PDGF-AA)[4]. However, excessive activation of CFs can drive pathological fibrosis and adverse cardiac remodeling, leading to impaired cardiac function and worsening post-infarction outcomes. Accordingly, most studies have focused on limiting CF activation[4]. More recently, however, the induction of senescence has emerged as a potential alternative strategy for mitigating post-MI damage[5].

Cellular senescence is characterized by irreversible cell proliferation arrest accompanied by distinct phenotypic alterations, such as the production of a senescence-associated secretory phenotype (SASP), typically induced in response to cellular stress or damage[6]. While most studies associate senescence with detrimental effects in chronic disease, it can have beneficial effects in acute disease contexts[6]. For example, senescent fibroblasts and endothelial cells have been shown to promote cutaneous wound healing by inducing myofibroblast differentiation[7]. Similarly, senescence of hepatic stellate cells (a fibroblast-like cell in the liver) protects against excessive liver fibrosis by halting proliferation, reducing production of ECM components, enhancing the secretion of ECM-degrading enzymes and promoting immune-mediated clearance[8]. Interestingly, senescent CFs have been found to significantly accumulate in infarct areas of the heart[9], and studies in p53-deficient mice showed fewer senescent CFs accompanied by increased cardiac collagen production following MI[9]. These findings suggest that fibroblast senescence may exert a protective role in the acute phase of MI. However, the mechanisms regulating the induction of fibroblast senescence following MI remain poorly understood.

Following activation, CFs exhibit increased metabolic demand and energy consumption. Mitochondria are central to cellular metabolism and Adenosine Triphosphate (ATP) production. During these processes, especially during aerobic metabolism, electron leakage from the mitochondrial electron transport chain reacts with oxygen to generate mitochondrial reactive oxygen species (mtROS)[10]. Mitochondrial dysfunction can further exacerbate Reactive Oxygen Species (ROS) production and result in the release of mitochondrial DNA, contributing to cellular damage and senescence.

Caspase recruitment domain-containing protein 10 (CARD10), a member of the caspase recruitment domain-containing and membrane-associated guanylate kinase-like (CARMA) protein family, is mainly expressed in non-hematopoietic tissues, including lung, kidney, and heart[11]. It has been implicated in maintaining mitochondrial integrity in liver sinusoidal endothelial cells after liver injury[12] and early studies have shown that its main effect is activating nuclear factor kappa-light-chain-enhancer of activated B cells (NF-κB) signaling[13]. Emerging evidence suggests that CARD10 functions extend beyond this pathway. For example, CARD10 has been reported to attenuate pulmonary fibrosis by reducing inflammation, collagen fiber deposition, and alveolar epithelial cell damage[14]. Our group has previously demonstrated that CARD10 deficiency exacerbates abdominal aortic aneurysm formation in angiotensin II-treated mice, which may be associated with increased pyroptosis and altered interaction between endoplasmic reticulum stress and mitochondrial damage[15]. Although previous studies have explored the role of CARD10 in diverse biological processes, its role in cardiac pathophysiology remains incompletely understood. Given its high expression in cardiac tissue, CARD10 represents an excellent candidate for investigation in the context of MI.

Here, we used CARD10 knockout (*Card10*$^{-/-}$) and wild-type (WT) mice to investigate cardiac function and fibroblast senescence following MI. In addition, primary CFs were isolated to assess senescence and damage in response to TGF-β stimulation. Through this approach, we aim to elucidate the role of CARD10 in post-MI remodeling and explore its potential as a novel therapeutic target for MI.

MATERIALS AND METHODS

Human sample collection and mouse model establishment

Human cardiac tissue samples were obtained from patients with MI undergoing heart transplantation at Nanjing First Hospital. Inclusion criteria: adult patients (≥ 18 years) undergoing orthotopic heart transplantation; diagnosis of end-stage ischemic cardiomyopathy secondary to previous myocardial infarction or coronary artery disease; availability of left ventricular myocardial tissue for analysis. Exclusion criteria: non-ischemic cardiomyopathy; active infection or systemic inflammatory disease; malignant tumors; autoimmune diseases; incomplete clinical information. Regions of the left ventricle exhibiting marked wall thinning and obvious white fibrosis were defined as the infarct zone, areas 1-2 cm adjacent to the infarct were defined as the border zone, and regions approximately 3 cm away without apparent wall thinning or white fibrosis were defined as the remote zone. Immediately after surgical excision, tissue specimens were dissected into small pieces (1 cm × 1 cm × 0.5 cm) according to the anatomical location and pathological lesion, fixed in 10% neutral-buffered formalin, dehydrated, embedded in paraffin, and stored as formalin-fixed paraffin-embedded (FFPE) blocks at room temperature. For histological analysis, paired myocardial tissue samples were obtained from both the infarct border zone (MI sample) and the remote non-infarcted zone (normal tissues) of each explanted heart. The study was conducted in accordance with the Declaration of Helsinki (revised in 2013) and was approved by the Ethics Committee of Nanjing First Hospital, Nanjing Medical University (04/04/2019, KY20190404-030KS-01). Prior to study participation, written informed consent was obtained from every patient.

Homozygous CARD10-deficient (*Card10*$^{-/-}$) mice with a C57BL/6 genetic background were kindly supplied by the Lin Xin Laboratory, Tsinghua University. WT mice of the same genetic background were purchased from GemPharmatech (Nanjing, China). Experimental MI was in 8-week-old male C57BL/6 mice using an

established surgical procedure. Animals were randomly assigned to the indicated groups. No formal sample size calculation was performed. Sample sizes were selected based on previous studies and our laboratory experience. No animals or samples were excluded unless death occurred before completion of the experimental protocol. Following induction of anesthesia with isoflurane (5%, 1 L/min), the animals underwent left thoracotomy for ligation of the left anterior descending coronary artery (LAD) under microscopic guidance. Mice in the sham group underwent an identical surgical procedure except for LAD ligation. Following surgery, mice received postoperative analgesia with buprenorphine (0.05-0.1 mg/kg, subcutaneously) and were monitored daily for signs of pain or distress. Animals were monitored daily for body weight, wound healing, activity, and general health throughout the study. The study was approved by the Experimental Animal Ethics Committee of Nanjing First Hospital, Nanjing Medical University (DWSY-24180857). When euthanasia was required, mice were subjected to isoflurane inhalation (5%, 5 L/min) followed by exposure to an overdose of CO_2 until death was confirmed. A total of 88 mice were enrolled in the study. One mouse died from causes unrelated to the experimental procedures, and the remaining 87 mice were included in the study. All analyses, such as histological, immunofluorescence, western blot, and so on, were performed by investigators blinded to the treatment groups.

Western blot

When testing heart tissue, whole heart lysis was used. Lysis of tissue and cell samples was performed on ice using Radioimmunoprecipitation Assay buffer (RIPA) buffer supplemented with protease and phosphatase inhibitor cocktail (20109ES05, YEASEN, China), and protein concentrations were quantified using a bicinchoninic acid (BCA) assay kit (KGP902, KeyGEN Biotech, China). Equal amounts of protein were separated by Sodium Dodecyl Sulfate-Polyacrylamide Gel Electrophoresis (SDS-PAGE) and subsequently transferred onto polyvinylidene fluoride (PVDF) membranes (Millipore, USA). After blocking with 5% bovine serum albumin (BSA) prepared in Phosphate-Buffered Saline (PBS) for 1 h at room temperature, the membranes were incubated overnight at 4 °C with primary antibodies diluted in 3% BSA. Following antibodies were used: p-histone H2A.X (1:1000, 2557, Cell Signaling Technology, USA), CARD10 (1:1000, ab137383, Abcam, UK); p16 (1:1000, ab51243, Abcam, UK); glyceraldehyde 3-phosphate dehydrogenase (GAPDH) (1:5000, 8884, Cell Signaling Technology, USA); protein kinase B (AKT) (1:1000, 9272, Cell Signaling Technology, USA); p-AKT (1:1000, 4060, Cell Signaling Technology, USA); phosphoinositide 3-kinase (PI3K) (1:1000, 4292, Cell Signaling Technology, USA); and p-PI3K (1:1000, 17366, Cell Signaling Technology, USA). Following three Tris-Buffered Saline with Tween 20 (TBST) washes, membranes were exposed to Horseradish Peroxidase (HRP)-conjugated secondary antibodies prepared in 1% BSA for 1 h at room temperature. Anti-rabbit IgG (1:8000, #7074, CST, USA) or anti-mouse IgG (1:8000, #91196, CST, USA) was selected according to the primary antibody used. Protein bands were developed using Immobilon® UltraPlus Western HRP Substrate (WBULP-100ML, Millipore, USA) and subsequently detected with an automatic chemiluminescence imaging analysis system (3300 Mini, Clinx Science Instruments, China). Densitometric analysis of protein bands was performed using NIH ImageJ software (NIH, USA).

Histology analysis

After fixation in 4% formalin for 24 h, cardiac tissues were processed through graded ethanol dehydration, infiltrated with paraffin and sectioned into 4-μm-thick slices. Histological examination was performed using hematoxylin and eosin (HE) and Masson's trichrome staining for evaluation of cardiac structural alterations and collagen deposition using light microscopy.

2,3,5-triphenyltetrazolium chloride staining

2,3,5-triphenyltetrazolium chloride (TTC) staining was used to determine the extent of tissue infarct areas. Fresh tissue samples were frozen at -80 °C for 10 min and subsequently sliced into 1 mm sections. The tissue samples were then immersed in 1% TTC (T8877-5G, MilliporeSigma, USA) in saline at 37 °C for 15 min and observed under a light microscope.

Table 1. Oligonucleotide primers used in this study

	Forward	Reverse
Pdgfa	GTCCACCACCGCAGTGTCAAG	CTACGCCTTCCTGTCTCCTCCTC
Tnfa	ACGGCATGGATCTCAAAGAC	AGATAGCAAATCGGCTGACG
Il6	ACAACGATGATGCACTTGCAGA	GATGAATTGGATGGTCTTGGTC

Immunofluorescence staining

For immunofluorescence (IF) staining, tissue samples embedded in Optimal Cutting Temperature (OCT) compound were sectioned at a thickness of 5 μm. The tissue sections were sequentially fixed with 4% paraformaldehyde, permeabilized using 0.5% Triton X-100, and blocked with goat serum (ZLI-9022, Beijing Zhongshan Biotechnology, China) before overnight incubation with primary antibodies at 4 °C. Cultured cells underwent the same staining procedure, with the exception of OCT embedding and cryosectioning. Following antibodies were used: CARD10 (1:100, ab137383, Abcam, UK); alpha-smooth muscle actin (α-SMA) (1:100, A5228, Sigma, USA); von Willebrand factor (VWF) (1:100, ab11713, Abcam, UK); troponin I (1:100, ab47003, Abcam, UK); p16 (1:1000, ab51243, Abcam, UK); vimentin (1:100, 5741, CST, USA). Samples were washed and further incubated with Alexa Fluor™ 488 chicken anti-rabbit IgG (H+L) (1:5000, A21441, Invitrogen, USA) or F(ab')2-Goat anti-Mouse IgG (H+L) Cross-Adsorbed Secondary Antibody, Alexa Fluor™ 546 (1:5000, 11018, Invitrogen, USA) for 1 h at room temperature. Cell nuclei were visualized by Hoechst (B-2261, Sigma, USA) staining. Images were captured using a fluorescence microscope (ZEISS SCOPE.A1, Germany).

Immunohistochemistry staining

For Immunohistochemistry (IHC) staining, tissue samples were embedded in 4% paraformaldehyde and sliced into 4-μm-thick sections. Following xylene deparaffinization and stepwise ethanol rehydration, paraffin sections underwent heat-induced antigen retrieval in citrate buffer (pH 6.0). Endogenous peroxidase was quenched by treatment with 3% hydrogen peroxide before nonspecific binding sites were blocked with normal serum. The sections were subsequently incubated with the appropriate primary antibodies against CARD10 (1:100; ab137383, Abcam, Cambridge, UK) overnight at 4 °C. After three rinses with PBS, the sections were incubated with an HRP-labeled polymer detection reagent (KIT-5004, MXB Biotechnologies, Fuzhou, China). Immunostaining was developed using a 3,3'-diaminobenzidine (DAB) detection kit (ZLI-9018, Beijing Zhongshan Biotechnology Co., Ltd., Beijing, China), followed by hematoxylin nuclear counterstaining. Representative images were acquired using a light microscope.

Echocardiographic analysis

Cardiac function was assessed four weeks after MI induction by echocardiography. Ejection fraction (EF), fractional shortening (FS), left ventricular internal diameter at end-diastole (LVIDd), and left ventricular internal diameter at end-systole (LVIDs) were measured with a Vevo2100 micro-ultrasound system equipped with a 30 MHz transducer (Visual-Sonics, Toronto, ON).

Real-time quantitative polymerase chain reaction

Gene expression was analyzed by real-time quantitative Polymerase Chain Reaction (qPCR) following an established protocol[15]. Total RNA was extracted from heart tissues or cells using TRIzol Reagent (15596-026, Invitrogen, USA), and cDNA was generated by Hifair III 1st strand cDNA synthesis superMix (11141ES60, YEASEN, China). qPCR was performed using Hieff UNICON Universal Blue qPCR SYBR Green Master Mix (1184ES08, YEASEN, China). All primer information is summarized in Table 1. The relative Ct (ΔΔCt) was calculated as $\Delta\Delta Ct = 2^{-(\Delta Ct\ MI - \Delta Ct\ CONTROL)}$, where $\Delta Ct = (Ct_{GENE} - Ct_{GAPDH})$ for each MI and control conditions;

Primary CF isolation

Primary CFs were isolated from 4-week-old mice as previously described. Briefly, hearts were quickly excised and washed in PBS. After being dissected into fragments of about 1 mm, the tissue was enzymatically digested in Hank's balanced salt solution (HBSS) supplemented with 0.6 mg/mL collagenase type II (C2-BIOC, Sigma, USA), 0.2 mg/mL collagenase type IV (C4-BIOC, Sigma, USA), and 0.2 mg/mL BSA (BS114-250g, Biosharp, China) for 10 min at 37 °C for enzymatic dissociation. This digestion step was repeated 4-5 times until the tissue fragments became noticeably smaller. Undigested tissue debris was removed by passing the suspension through a 40-μm filter. Erythrocytes were removed using red blood cell lysis buffer (C3702-500 mL, Beyotime, China). The filtrate was centrifuged for 10 min at 1,000 rpm and the resulting pellet was resuspended in DMEM/F12 (11320033, Gibco, USA) supplemented with 1% penicillin-streptomycin (P4333-100ML, Sigma, USA) and 10% fetal bovine serum (A5670502, Gibco, USA). Only cell preparations with > 80% vimentin-positive cells were used for subsequent experiments. All experiments were conducted using cells at passage 2-3.

Wound healing assay

Human umbilical vein endothelial cells (HUVEC) were kindly provided by the Clinical Medicine Research Center in Nanjing Drum Tower Hospital [16]. Cell identity had been routinely authenticated before use. HUVECs were cultured in ECM medium [500 mL of basal medium (1001, Solarbio life science, China), 25 mL of fetal bovine serum (0025, Solarbio life science, China), 5 mL of endothelial cell growth supplement (1052, Solarbio life science, China) and 5 mL of penicillin/streptomycin solution (0503, Solarbio life science, China)] to confluence in 6-well plates. All experiments were conducted using cells at passages 3-5. Cells were scratched with a sterile 10-μL pipette tip, washed with PBS, and incubated in conditioned medium. The conditioned medium was prepared by mixing the supernatant of CF cultures with DMEM/F12 (10% FBS) at a 1:1 ratio. Three areas in each well were randomly selected under a light microscope (IX73, Olympus, Japan). The cell migration rate was calculated as: Cell migration rate = $(L_0 - L_t)/L_0$*100%, where L_0 represents the scratch width at 0 h and L_t represents the scratch width at 24 h[17].

Tube formation assay

HUVECs (3.5×10^5 cells/well) were seeded onto Matrigel (356234, Corning, USA) -coated 96-well plates for tube formation. HUVECs were then incubated with 100 μL of conditioned medium per well at 37 °C for 6 h in humidified atmosphere. The conditioned medium was prepared by mixing the supernatant of CF cultures with ECM medium (same as wound healing assay) at a 1:1 ratio. Images were acquired using a light microscope (IX73, Olympus, Japan) and analyzed with the ImageJ Angiogenesis analyzer plugin[18].

Mitochondrial integrity

Mitochondrial membrane potential was assessed using a JC-1 staining kit (C2003S, Beyotime, China). Following PBS washing, CFs were then incubated with JC1 working solution at 37 °C for 20 min. Mitochondrial membrane potential (ΔΨm) was evaluated by calculating the fluorescence intensity ratio of aggregated (red) to monomeric (green) JC-1. JC-1 aggregates were measured at excitation/emission wavelengths of 585/590 nm, and JC-1 monomers were measured at 514/529 nm.

Superoxide was measured using MitoSOX staining (M36008, thermofisher, USA). MitoSOX Red reagent was dissolved in anhydrous Dimethyl Sulfoxide (DMSO) and subsequently diluted in HBSS containing calcium and magnesium to obtain a final working concentration of 500 nM. After being washed with PBS, CFs were treated with the MSR working solution at 37 °C for 30 min under light-protected conditions. Fluorescence signals were measured at excitation/emission wavelengths of 396/610 nm.

Transmission electron microscopy (TEM) was used to examine Cellular ultrastructure. Following fixation in 2.5% glutaraldehyde and postfixation with osmium tetroxide, cell samples were dehydrated in a graded

ethanol series and infiltrated with epoxy resin. Ultrathin sections were prepared for uranyl acetate and lead citrate staining prior to TEM imaging.

Statistical analysis

PCR, western blot, and migration assay data are shown as mean ± Standard Error of the Mean (SEM). Comparisons among three or more groups were performed using two-way Analysis of Variance followed by Sidak's multiple comparisons test. All statistical analyses were conducted using GraphPad Prism 8.02 (GraphPad Software, San Diego, CA, USA). Results were considered statistically significant when $P < 0.05$.

RESULTS

Increased expression of CARD10 in heart tissue after MI and co-localization with a-SMA in CFs

To investigate the expression and localization of CARD10 following MI, Western blot and IHC staining were performed to compare CARD10 levels between MI and sham-operated mice. CARD10 expression was found elevated in whole heart lysates from MI mice. Expression was found highest at one week after MI induction [Figure 1A and B]. IHC staining of mouse heart tissue one week following MI induction confirmed elevated CARD10 expression [Figure 1C and D]. IF staining showed that CARD10 colocalized with the fibroblast marker α-SMA in a scattered pattern around the border zone of infarcted mouse hearts [Figure 1E]. Additionally, comparable results were found in human heart samples by IHC staining of CARD10 [Figure 1F and G]. Baseline characteristics of the volunteers are in Table 2. These results suggest that CARD10 may contribute to the pathophysiology of MI, potentially through its involvement in CFs.

CARD10 deficiency attenuates myocardial injury

To investigate the role of CARD10 in MI, MI was induced by LAD coronary artery ligation in *Card10*$^{-/-}$ and WT mice. Echocardiography and sample collection for morphological analyses were carried out four weeks after surgery. Heart tissue from *Card10*$^{-/-}$ mice exhibited a lower degree of fibrosis compared to heart tissue from WT mice, as assessed by HE and Masson staining [Figure 2A-D]. TTC staining revealed smaller infarct areas in heart tissue from *Card10*$^{-/-}$ mice [Figure 2E and F]. Echocardiographic analysis [Figure 2G and H] revealed significantly restored cardiac function in *Card10*$^{-/-}$ mice compared to WT mice after MI induction, with higher EF and FS and decreased LVIDd and LVIDs. Reduced heart weights were observed in *Card10*$^{-/-}$ mice after MI induction. Furthermore, increased expression of the endothelial cell marker VWF [Figure 2I and J] and the smooth muscle cell marker a-SMA [Figure 2K and L] was found in the cardiac tissue of *Card10*$^{-/-}$ mice compared to WT mice after MI induction. This indicates increased angiogenic capacity in mice deficient in CARD10. Collectively, these results of the morphological and functional analyses suggest that CARD10 deficiency attenuates the effects of MI.

CARD10 deficiency promotes CF senescence

Previous studies have suggested that CF senescence may exert beneficial effects following MI[5]. To assess cellular senescence in our experimental model and the effects of CARD10 deficiency, an SA-β-gal activity assay was performed in heart tissue one week after MI induction. We found an accumulation of SA-β-gal staining in regions adjacent to the infarct area of hearts from *Card10*$^{-/-}$ mice that was absent in hearts from WT mice [Figure 3A]. In addition, the expression of senescence markers p16 and phosphorylated histone H2A.X (p-histone H2A.X) was examined using Western blot analysis [Figure 3B and C]. Both markers were expressed at significantly higher levels in *Card10*$^{-/-}$ mouse tissue following MI. These results indicate an increased level of senescence in the infarcted hearts of *Card10*$^{-/-}$ mice.

To further validate these findings in vitro, primary CFs were isolated from *Card10*$^{-/-}$ and WT adult mice and were stimulated with TGF-β (10 ng/mL) for 4 days to establish a senescence model. The *Card10*$^{-/-}$ CFs stimulated with TGF-β showed increased SA-β-gal activity compared with WT CFs [Figure 3D]. Consistent

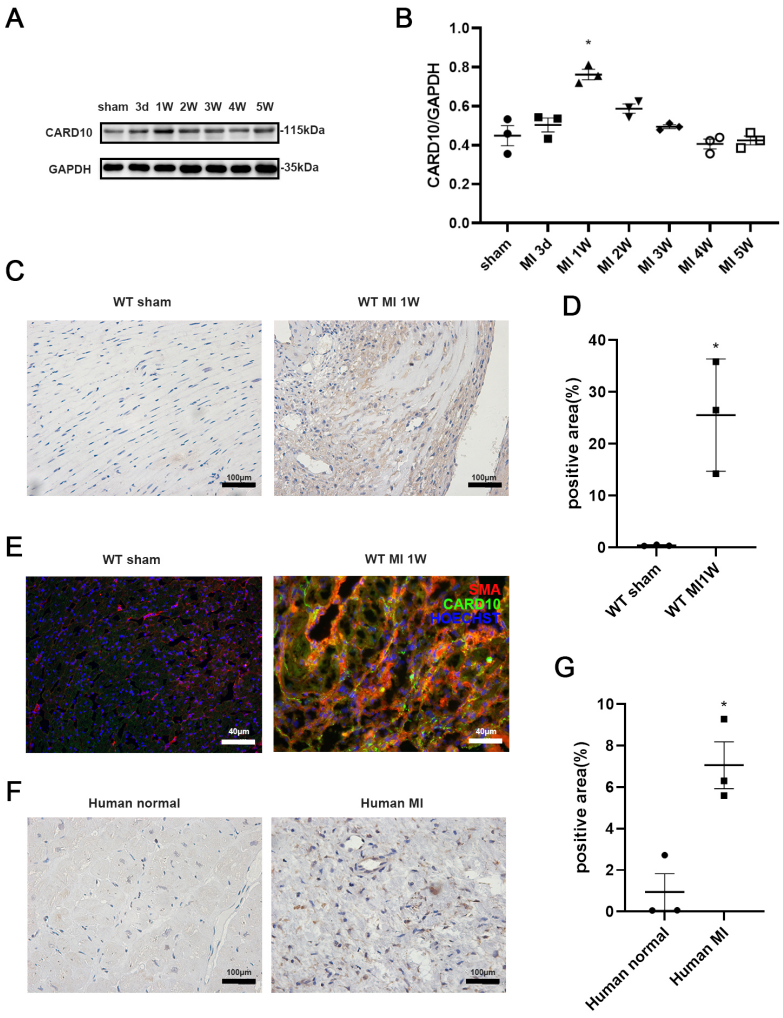

Figure 1. Increased CARD10 expression in heart tissues after MI induction. Western blot (A) (biological replicates $n = 3$, technical replicates 1) and densitometric analysis (B) in mouse whole heart lysates three days (3d) and one to five weeks (1 W to 5 W) after MI induction. CARD10 expression was highest one week after MI induction. ($n = 3$ per group); Representative images (C) and analysis (D) of IHC staining for CARD10 (biological replicates $n = 3$, technical replicates 1) in mouse heart one week after MI. Objective: 10×; (E) IF staining (biological replicates $n = 3$, technical replicates 1) showing scattered distribution of CARD10 and co-localization with a-SMA in infarcted heart tissue 1 week after MI, indicating predominant expression in CFs. Objective: 20×; Representative images (F) and analysis (G) of IHC staining for CARD10 (biological replicates $n = 3$, technical replicates 1) in human MI tissue. Objective: 10×. Differences in CARD10 expression among multiple groups were analyzed using one-way ANOVA. Comparisons between two groups were performed using the Mann-Whitney *U* test. * $P < 0.05$. CARD10: Caspase recruitment domain-containing protein 10; MI: myocardial infarction; IHC: Immunohistochemistry; IF: immunofluorescence; α-SMA: α-smooth muscle actin; CFs: cardiac fibroblasts; ANOVA: analysis of variance; WT: wildtype.

Table 2. Baseline characteristics of the participants

	Participant 1	Participant 2	Participant 3
Age	66	44	57
Sex	Male	Female	Female
Smoke	Yes	No	No
Diabetes	Yes	No	No
Time from MI to heart transplantation	5 months	5 months	11 days
NYHA class#	IV	IV	IV

NYHA: New York Heart Association. MI: Myocardial infarction.

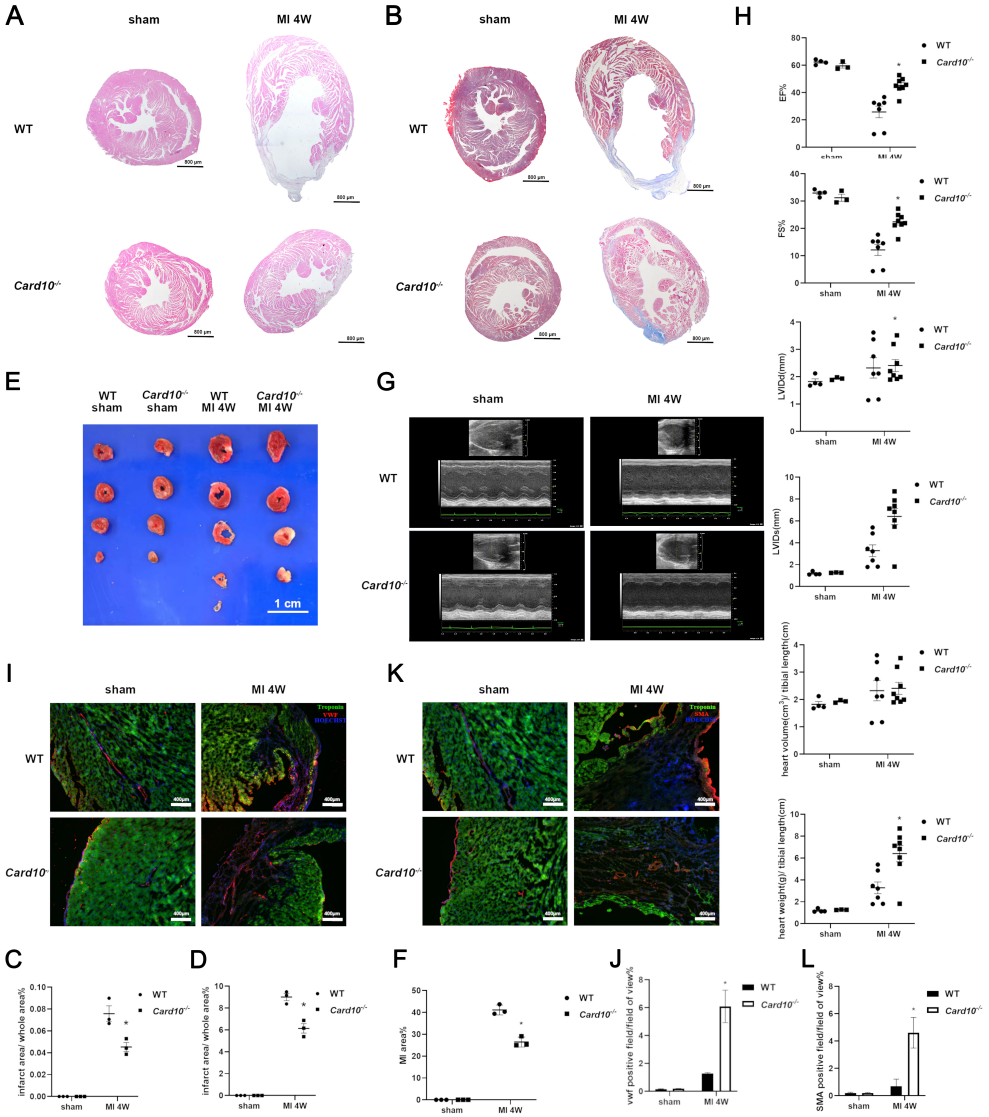

Figure 2. CARD10 deficiency attenuated cardiac fibrosis and improved heart function and angiogenesis following MI. Representative images of HE (A) and Masson staining (B), with their respective analyses (C and D, respectively), of cardiac tissue obtained from *Card10*$^{-/-}$ and WT mice four weeks after MI or sham surgery (biological replicates n = 3, technical replicates 1). TTC staining (E) and its analysis (F) of cardiac tissue obtained from *Card10*$^{-/-}$ and WT mice four weeks after MI or sham surgery (biological replicates n = 3, technical replicates 1). Echocardiography was performed using the Vevo2100 micro-ultrasound system at 4 weeks after MI. Echocardiographic analysis: representative parasternal long-axis views and M-mode images (G) and quantification (H) of EF, FS, LVIDd, LVIDs, heart weight, and heart volume normalized by tibial length 4 weeks after MI or sham operation in *Card10*$^{-/-}$ and WT mice (WT control: n = 4; *Card10*$^{-/-}$ control: n = 3; WT MI: n = 7; *Card10*$^{-/-}$ MI: n = 8). Representative IF staining of cardiomyocyte marker troponin I and endothelial cell marker VWF (I), with its corresponding quantification (J), or of cardiomyocyte marker troponin I and vascular smooth muscle cell marker α-SMA (K), with its corresponding quantification (L), in cardiac tissue obtained from *Card10*$^{-/-}$ and WT mice 4 weeks after MI or sham surgery (biological replicates n = 3, technical replicates 1). Objective: 10×. Data are expressed as mean ± SEM. Comparisons between different groups were performed using the two-way ANOVA followed by Šídák's multiple comparisons test. *P < 0.05 WT MI *vs.* *Card10*$^{-/-}$ MI. CARD10: Caspase recruitment domain-containing protein 10; MI: myocardial infarction; HE: hematoxylin and eosin; TTC: triphenyltetrazolium chloride; WT: wildtype; EF: ejection fraction; FS: fractional shortening; LVIDd: left ventricular internal diameter at end-diastole; LVIDs: left ventricular internal diameter at end-systole; IF: immunofluorescence; VWF: von Willebrand factor; α-SMA: α-smooth muscle actin; SEM: standard error of the mean; ANOVA: analysis of variance.

with this observation, Western blot analysis demonstrated significantly higher expression of p16 and p-histone H2A.X in the *Card10*$^{-/-}$ CFs upon TGF-β stimulation [Figure 3E and F]. IF staining further confirmed an increased number of p16-positive *Card10*$^{-/-}$ CFs after TGF-β stimulation [Figure 3G]. These in vitro results are consistent with the *in vivo* findings, confirming enhanced senescence in *Card10*$^{-/-}$ cells, consistent with

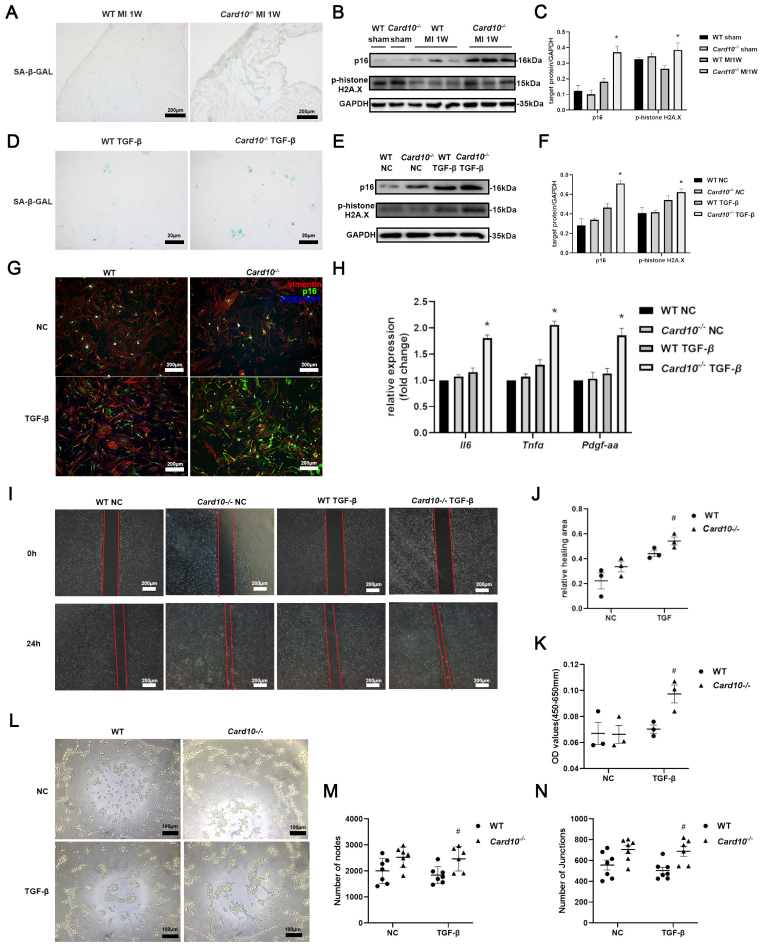

Figure 3. CARD10 deficiency induced CF senescence. (A) Representative images of SA-β-gal staining (biological replicates *n* = 3, technical replicates 1) showing increased SA-β-gal signal in cardiac tissue obtained from *Card10*$^{-/-}$ and WT mice one week (1 W) after MI surgery. Objective: 10×; (B) Western blot (biological replicates *n* = 3, technical replicates 2) and (C) densitometric analysis showing that senescence markers p16 and p-histone H2A.X were more abundant in *Card10*$^{-/-}$ MI mice heart compared to WT MI; (D) Representative images of SA-β-gal staining of CFs (biological replicates *n* = 3, technical replicates 1) obtained from *Card10*$^{-/-}$ and WT adult mice after TGF-β stimulation. Objective: 20×; (E) Western blot (p16: biological replicates *n* = 3, technical replicates 1, p-histone H2A.X: biological replicates *n* = 2, technical replicates 2) and (F) densitometric analysis showing that senescence markers p16 and p-histone H2A.X were more abundant in CFs obtained from *Card10*$^{-/-}$ and WT adult mice after TGF-β stimulation. NC, negative control; (G) Representative IF staining (biological replicates *n* = 3, technical replicates 1) showing colocalization of CF marker vimentin and p16 in primary CFs isolated from *Card10*$^{-/-}$ and WT adult mice after TGF-β stimulation. Objective: 10×; (H) RT-qPCR analysis (biological replicates *n* = 3, technical replicates 3) of senescence-associated secretory phenotype factors *Il6, Tnfa,* and *Pdgfa* in primary CFs isolated from *Card10*$^{-/-}$ and WT adult mice after TGF-β stimulation. Then HUVECs were cultured in conditioned medium derived from *Card10*$^{-/-}$ or WT cardiac fibroblasts treated with TGF-β for 4 days. Wound healing assay (biological replicates *n* = 3, technical replicates 1) (I) and quantitative analysis (J) were used to determine HUVEC migration. Objective: 10×. NC, negative control (no stimulation of CFs with TGF-β); CCK8 assay (biological replicates *n* = 3, technical replicates 3) (K) was used to determine HUVEC proliferation; Representative images of the tube formation assay (*Card10*$^{-/-}$ TGF-β group biological replicates *n* = 3, technical replicates 2, other group biological replicates *n* = 3, technical replicates 4) (L) and quantitative analysis of nodes (M) and junctions (N) showed more angiogenesis in HUVECs cultured with *Card10*$^{-/-}$ CF-derived conditioned medium compared to HUVECs cultured with WT CF-derived conditioned medium. Comparisons between different groups were performed using the two-way ANOVA followed by Šídák's multiple comparisons test. * $P < 0.05$ WT MI *vs. Card10*$^{-/-}$ MI, or WT TGF-β *vs. Card10*$^{-/-}$ TGF-β. # $P < 0.05$ WT conditioned medium *vs. Card10*$^{-/-}$ conditioned medium. CARD10: Caspase recruitment domain-containing protein 10; CFs: cardiac fibroblasts; WT: wildtype; MI: myocardial infarction; TGF -β: transforming growth factor-beta; IF: immunofluorescence; RT-qPCR: real-time quantitative polymerase chain reaction; HUVECs: human umbilical vein endothelial cells; ANOVA: analysis of variance; SA-β-gal: senescence-associated β-galactosidase.

the *in vivo* results. Senescent cells are known to develop a SASP, characterized by the release of proinflammatory factors such as Interleukin-6 (IL-6), Tumor Necrosis Factor-alpha (TNF-α), and Platelet-Derived Growth Factor-AA (PDGF-AA)[19]. The expression of these factors was assessed by Real-time

quantitative polymerase chain reaction (RT-qPCR). Following TGF-β stimulation, *Card10*$^{-/-}$ CFs exhibited significantly higher mRNA levels of *Il6, Tnf,* and *Pdgfa* compared with WT CFs [Figure 3H]. Collectively, these results indicated that CARD10 deficiency promotes a pronounced senescence phenotype in the heart.

We have previously demonstrated that CARD10 deficiency promotes angiogenesis following MI [Figure 2I-L]. To investigate whether this effect is due to factors released by senescent cells, the effects of CF-derived conditioned medium on migration, proliferation, and angiogenesis of HUVECs were determined. The conditioned medium was prepared by combining the supernatant of *Card10*$^{-/-}$ or WT CFs incubated with TGF-β for 4 days with DMEM (10% FBS) at a 1:1 ratio.

HUVECs cultured with *Card10*$^{-/-}$ CF-derived conditioned medium exhibited significantly higher migration and proliferation compared with HUVECs cultured with WT CF-derived conditioned medium, as determined by healing [Figure 3I and J] and CCK8 assay [Figure 3K]. Moreover, under the same conditions, HUVECs produced significantly more nodes and junctions as determined in a tube formation assay [Figure 3L-N]. Collectively, these results indicate that senescent fibroblasts promote endothelial cell proliferation and activities that contribute to attenuating the damage associated with MI. This effect may be mediated by secretion of SASP factors, including PDGF-AA.

For the rescue experiment, we used quercetin (10 μM, HY-18085, MedChemExpress, NJ, USA) to anti-senescence for 48 h[20] to treat CFs. p16 was decreased after quercetin stimulation [Supplementary Figure 1A and B], validating that senescence was alleviated after quercetin stimulation. Then, HUVECs were cultured with CF-derived conditioned medium. The pro-angiogenic effects of *Card10*$^{-/-}$ CF-derived conditioned medium on HUVECs were partially diminished [Supplementary Figure 1C-G], implicating that the cardioprotective effects associated with CARD10 deficiency may be mediated by fibroblast senescence.

Mitochondrial dysfunction in CARD10 deficient CFs is mediated by the AKT/PI3K signaling pathway

Mitochondrial dysfunction is a well-established hallmark of cellular senescence. We therefore investigated the contribution of mitochondrial dysfunction to the senescence phenotype induced by CARD10 deficiency in CFs isolated from *Card10*$^{-/-}$ and WT adult mice following stimulation with TGF-β. Mitochondrial membrane potential, mtROS production and mitochondrial ultrastructure were assessed by JC-1 staining, MitoSOX Red fluorescence and TEM, respectively. Upon stimulation with TGF-β, *Card10*$^{-/-}$ CFs exhibited significantly lower mitochondrial membrane potential compared to WT CFs [Figure 4A and B] but generated significantly more mtROS [Figure 4C and D]. TEM analysis showed mitochondrial ultrastructural abnormalities in WT CFs stimulated with TGF-β that were further aggravated in *Card10*$^{-/-}$ CFs [Figure 4E]. These findings indicate that CARD10 deficiency exacerbated mitochondrial damage after TGF-β stimulation.

Given the established role of the PI3K/AKT signaling pathway in both mitochondrial dysfunction and cellular senescence, we next examined its activation status. Notably, phosphorylation of both PI3K and AKT was significantly increased in TGF-β-stimulated *Card10*$^{-/-}$ CFs compared to WT CFs [Figure 4F and G], suggesting that the PI3K/AKT pathway may contribute to CARD10-mediated regulation of CF senescence.

DISCUSSION

MI is a life-threatening cardiovascular disease[3]. Despite advances in clinical management that have improved survival rates, many patients continue to experience adverse outcomes following MI, including arrhythmias, cardiac remodeling, and heart failure[21]. CFs are key regulators in cardiac remodeling and play a central role in the development of post-infarction fibrosis[22]. Our previous study demonstrated that CARD10 deficiency attenuates the development of bleomycin-induced pulmonary fibrosis[14]. However, whether

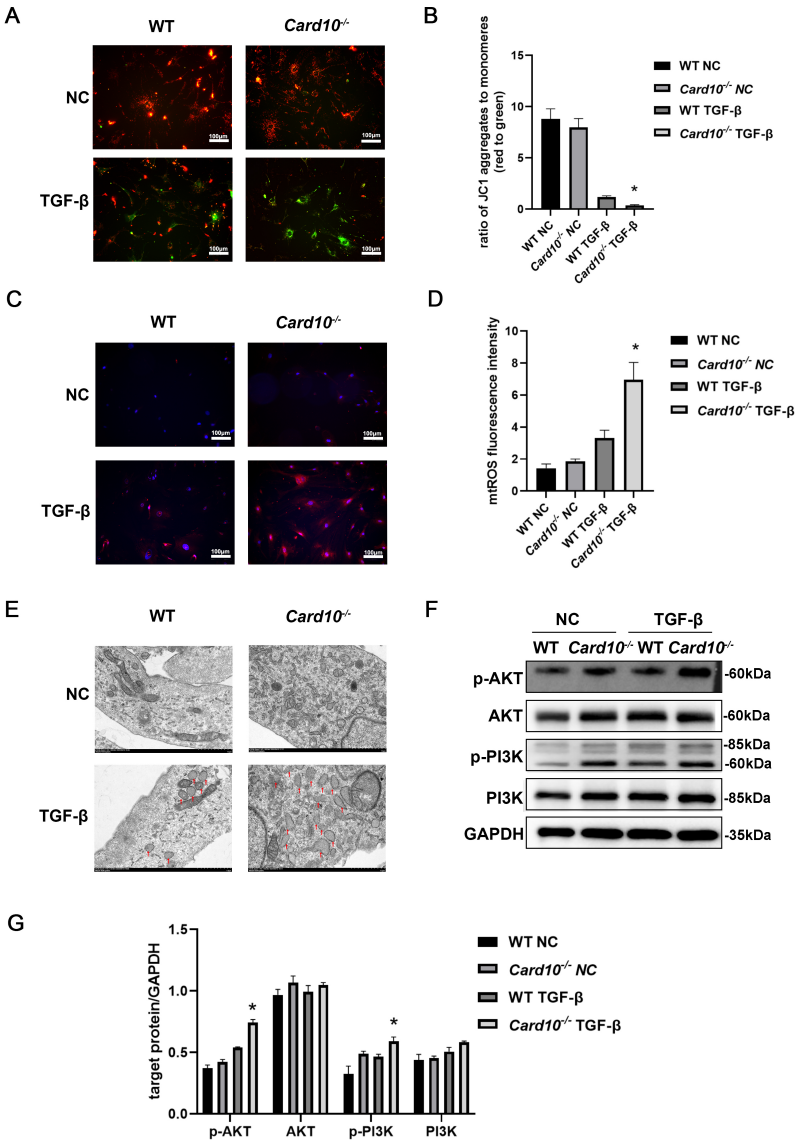

Figure 4. CARD10 deficiency aggravates mitochondrial dysfunction by activating the AKT/PI3K signaling pathway. The assays were conducted in CFs isolated from *Card10*$^{-/-}$ and WT adult mice and stimulated with TGF-β. Representative images of JC-1 staining (biological replicates n = 3, technical replicates 1) (A) and quantification of JC-1 levels (B); NC, negative control. Objective: 10×. Representative images (C) and quantification of MitoSOX Red fluorescence intensity (biological replicates n = 3, technical replicates 1) (D) for determination of mtROS levels. Objective: 10×; (E) Mitochondrial morphology was assessed by TEM (biological replicates n = 2, technical replicates 2). Scale bars: 1 μm. Western blot (p-PI3K&PI3K: biological replicates n = 3, technical replicates 2, p-AKT&AKT: biological replicates n = 3, technical replicates 2) (F) and densitometric analysis (G) showed increased levels of p-AKT and p-PI3K expressed in cell lysates of CFs isolated from *Card10*$^{-/-}$ adult mice and stimulated with TGF-β. Comparisons between different groups were performed using the two-way ANOVA followed by Šídák's multiple comparisons test. * $P < 0.05$ *Card10*$^{-/-}$ TGF-β *vs.* WT TGF-β. CARD10: Caspase recruitment domain-containing protein 10; AKT: protein kinase B; PI3K: phosphoinositide 3-kinase; CFs: cardiac fibroblasts; WT: wildtype; MI: myocardial infarction; TGF-β: transforming growth factor-beta; IF: immunofluorescence; mtROS: mitochondrial reactive oxidative species; TEM: transmission electron microscopy.

CARD10 contributes to cardiac fibrosis following MI remains unclear. Therefore, the present study aimed to investigate the role of CARD10 in post-MI cardiac remodeling using both *in vivo* and in vitro models, and to elucidate the molecular mechanisms underlying its effects.

In the present study, we examined the expression and localization of CARD10 in heart tissue following MI and found that CARD10 expression was markedly increased in the infarcted myocardium of mice. IF analysis revealed colocalization of CARD10 with α-SMA. α-SMA is expressed by both cardiac fibroblasts and

vascular smooth muscle cells, making definitive lineage identification based on this marker alone challenging[23,24]. However, vascular smooth muscle cells typically exhibit a concentric organization around endothelial cells within blood vessels. In contrast, CARD10-positive cells exhibited a scattered distribution pattern, suggesting that CARD10 expression is more likely associated with CFs than with vascular smooth muscle cells. Nevertheless, the use of additional fibroblast-specific markers would be necessary to further validate the cellular source of CARD10 expression. To assess the clinical relevance of these findings, we analyzed human cardiac tissue obtained from patients with MI undergoing heart transplantation. Consistent with our observations in the mouse tissue, CARD10 expression was significantly higher in the border zone compared to the remote zone of the myocardium. The concordance between the human and mouse results supports a potential role of CARD10 in the pathophysiological response to MI. Given its localization pattern and increased expression in infarcted tissue, CARD10 may contribute to post-infarction cardiac remodeling and fibrosis through its actions in CFs.

Post-MI remodeling is a dynamic process involving inflammation, fibroblast activation, ECM deposition, and angiogenesis, all of which collectively determine long-term ventricular function[25]. Adverse remodeling is associated with larger infarct areas, excessive fibrosis, ventricular dilation, impaired cardiac function, as reflected by reduced EF and FS[26], and increased heart weight, as observed in WT mice following MI. In contrast, CARD10 deficiency significantly attenuated post-MI cardiac dysfunction and structural remodeling. Given that neovessel formation promotes tissue repair, limits scar formation, and improves cardiac function following MI[27], the increased angiogenic response observed in *Card10*$^{-/-}$ MI mice may contribute to their improved cardiac outcomes. These results suggest that CARD10 deficiency mitigates cardiac remodeling and dysfunction after MI.

Recent studies have identified CF senescence as a potential therapeutic target for alleviating adverse cardiac remodeling following MI[5,9,28]. Although cellular senescence has detrimental effects in chronic diseases, accumulating evidence suggests that it may exert protective effects in acute injury settings, including cutaneous wounds and MI[9,29]. For example, Exercise has been shown to attenuate myocardial fibrosis by promoting fibroblast senescence[28]. Senescent fibroblasts undergo irreversible cell cycle arrest, thereby limiting excessive proliferation and protecting against myocardial fibrosis[9]. The sustained cell cycle arrest characteristic of senescent cells is accompanied by several well-established molecular and cellular markers, including elevated expression of cell cycle inhibitors $p21^{Cip1/Waf}$ and $p16^{Ink4a}$, activation of the DNA damage response pathway as indicated by gH2A.X, and elevated activity of the lysosomal enzyme SA-β-gal[30-32]. In the present study, *Card10*$^{-/-}$ mice exhibited significantly increased expression of senescence markers, including p16, p-histone H2A.X, and SA-β-gal activity following MI. Consistent with the *in vivo* findings, CARD10 deficiency promoted a senescence phenotype in TGF-β-stimulated CFs, a widely used model of fibroblast senescence[33], supporting a role for CARD10 as a negative regulator of cardiac fibroblast senescence.

Furthermore, senescent cells develop a SASP, characterized by the secretion of a wide range of cytokines and growth factors, including IL-6, TNF-α, and PDGF-AA[19,32]. Recent study has shown that vascular endothelial cells and brain-resident macrophages transiently exhibit pro-inflammatory senescence profiles during brain vascularization, with bidirectional signaling between these cell populations contributing to angiogenic patterning and extracellular matrix assembly[34]. In the present study, *Card10*$^{-/-}$ CFs were found to exhibit increased secretion of SASP factors compared with WT CFs. Among these factors, PDGF-AA is reported to promote endothelial cell recruitment and proliferation, thereby facilitating angiogenesis[7]. To investigate the functional consequences of the altered secretory profile of *Card10*$^{-/-}$ CFs, conditioned medium derived from CFs was applied to HUVECs. Notably, HUVECs exposed to *Card10*$^{-/-}$ CF conditioned medium displayed enhanced proliferative angiogenic capacities compared with those treated with conditioned media from WT CFs. While inhibiting CFs senescence, these effects were partially abolished. Given the established role of

angiogenesis in cardiac repair after MI, enhanced fibroblast senescence may represent one mechanism by which CARD10 deficiency attenuates post-infarction cardiac injury and adverse remodeling.

Cellular senescence is accompanied by widespread organelle dysfunction, with mitochondrial impairment among its most prominent hallmarks. Senescence-associated mitochondrial dysfunction is characterized by elevated production of ROS and 4-hydroxynonenal, lysosomal dysfunction, and impaired autophagosome flux[32,35]. Conversely, excessive ROS generation, dysregulated autophagy, and mitochondrial DNA damage can further aggravate mitochondrial dysfunction and promote cellular senescence[36,37]. In the present study, TGF-β-stimulated *Card10*$^{-/-}$ CFs were found to exhibit significantly elevated mtROS levels compared to WT CFs. Furthermore, CARD10 deficiency was associated with a reduction in mitochondrial membrane potential and more pronounced mitochondrial ultrastructure abnormalities, indicating exacerbated mitochondrial dysfunction. These findings suggest that CARD10 plays an important role in maintaining mitochondrial integrity in CFs under profibrotic conditions. Mitochondria serve as central metabolic hubs in fibroblasts, regulating ATP production, lipid and glucose metabolism, and calcium homeostasis[38]. Following MI, the altered cardiac microenvironment promotes rapid fibroblast proliferation and phenotypic transformation[4]. These changes are accompanied by increased mitochondrial oxidative phosphorylation, which can lead to electron leakage from the electron transport chain and subsequent mtROS generation, a potent driver of senescence[39]. Accumulating evidence suggests that mtROS may induce premature senescence through several mechanisms, including activation of the NOD-, LRR-, and pyrin domain-containing protein 3 (NLRP3) inflammasome, DNA damage, and upregulation of SASP pathways[36]. Consistent with these observations, increased mtROS levels have been linked to elevated expression of senescence markers such as p-histone H2A.X and p53, as well as persistent DNA damage responses that promote senescence[37]. Based on our findings, we propose that CARD10 deficiency enhances mtROS production and mitochondrial dysfunction, thereby promoting CF senescence. In turn, the senescent state may further impair mitochondrial function and increase ROS generation, establishing a positive feedback loop that reinforces both mitochondrial dysfunction and cellular senescence. This mechanism may contribute to the enhanced senescence phenotype observed in *Card10*$^{-/-}$ CFs. The PI3K-AKT signaling pathway is a central regulator of numerous cellular processes, including cell survival, proliferation, inflammation, and oxidative stress[40]. Although the PI3K/AKT pathway is classically recognized for its oncogenic functions, accumulating evidence suggests that its sustained or aberrant activation can also induce a senescence-like phenotype, a process referred to as oncogene-induced senescence[41-43], and antagonizing this pathway has been reported to promote autophagy and inhibit myofibroblast senescence[44]. Similarly, glucocorticoid-induced premature senescence in trabecular meshwork cells has been shown to be accompanied by activation of the PI3K/AKT/monoamine oxidase A (MAOA) pathway, mitochondrial dysfunction, and oxidative stress[45]. Consistent with these observations, we demonstrate enhanced activation of this pathway in *Card10*$^{-/-}$ CFs following TGF-β stimulation. Given the established role of PI3K/AKT signaling in regulating oxidative stress and mitochondrial homeostasis, these findings suggest that PI3K/AKT activation may contribute to the increased mtROS production, mitochondrial dysfunction, and senescence observed in *Card10*$^{-/-}$ CFs.

Several limitations of this study should be acknowledged. First, although the murine MI model recapitulates many key features of human disease, species-specific differences may limit the direct translation of our findings to clinical settings. Future studies employing more clinically relevant models, such as induced pluripotent stem cell (iPSC)-derived CFs, cardiac organoids, or non-human primate models, may help to further validate the role of CARD10 in human MI. Second, post-MI remodeling was evaluated only during a four-week observation period. Given the dynamic nature of cardiac remodeling, the impact of CARD10 may vary across different stages of disease progression. Longitudinal studies with extended follow-up periods will therefore be necessary to define the temporal contribution of CARD10 to post-infarction cardiac repair and

remodeling. Third, mitochondrial functional assessment was limited to TEM, JC-1 staining, and mtROS measurements. Although these approaches provide evidence of mitochondrial dysfunction, more comprehensive assessments of mitochondrial physiology, including mitochondrial respiration and ATP production, were not conducted. Fourth, inhibition/activation of the PI3K/AKT pathway as a rescue experiment was not performed; the mechanism is not fully clear. Fifth, all experiments were performed using young male mice. Therefore, potential age- and sex-related factors, which are known to influence cardiac remodeling, fibrosis and cellular senescence, were not evaluated. This may limit the generalizability of our findings. Future studies incorporating both sexes and multiple age groups will be important to determine whether the effects of CARD10 are modulated by age or sex. Finally, the mechanistic analyses presented in this study are largely observational. Moreover, inter-individual heterogeneity among human tissue samples may have influenced the observed results. Additional mechanistic studies and validation in larger human cohorts will be required to establish definitive causal relationships and further elucidate the role of CARD10 in post-MI cardiac remodeling.

Conclusion

This study identifies CARD10 as a novel regulator of cardiac fibroblast senescence and suggests that targeting it may represent a potential strategy to improve cardiac repair after MI. Importantly, given the context-dependent effects of cellular senescence, precise temporal control of senescence modulation will likely be required to maximize beneficial effects while minimizing adverse remodeling.

DECLARATIONS

Acknowledgments

Homozygous *Card10*$^{-/-}$ mice (C57BL/6 background) were provided by the Lin Xin Laboratory of Tsinghua University. HUVECs were a gift from the Clinical Medicine Research Center at Nanjing Drum Tower Hospital. Graphical Abstract created in BioRender. Xu Y (2026) https://BioRender.com/zq8obbq.

Authors' contributions

Performed the experiments: Xu Y, Yao Y, Zhou Y
Wrote the original draft and conducted data analysis: Xu Y
Participated in the animal model establishment: Chen G, Li W, Cao Y
Isolated the cardiac fibroblasts: Liu Y, Jiang Y, Cao X
Helped design the experiments and review the manuscript: Chen W, Chen X

Availability of data and materials

The datasets generated and/or analyzed during the current study are available from the corresponding author upon reasonable request.

AI and AI-assisted tools statement

During the preparation of this manuscript, the AI tool ChatGPT (version GPT-5.1, released 2025-11-12) was used solely for language editing. The tool did not influence the study design, data collection, analysis, interpretation, or the scientific content of the work. All authors take full responsibility for the accuracy, integrity, and final content of the manuscript.

Financial support and sponsorship

This study was supported by the National Natural Science Foundation of China [grant number: 82170272] and the Young Program of the National Natural Science Foundation of China [grant number: 82200529].

Conflicts of interest

All authors declared that there are no conflicts of interest.

Ethical approval and consent to participate

This study was conducted in accordance with the Declaration of Helsinki (revised in 2013). The study was

approved by the Ethics Committee of Nanjing First Hospital, Nanjing Medical University (KY20190404-030KS-01). All patients provided informed consent. The animal study was approved by the Experimental Animal Ethics Committee of Nanjing First Hospital, Nanjing Medical University (DWSY-24180857).

Consent for publication

Not applicable.

Copyright

Supplementary Materials

Supplementary Materials

REFERENCES

1. Di Cesare M, Perel P, Taylor S, et al. The heart of the world. *Glob Heart.* 2024;19:11. DOI PubMed PMC
2. 2017 Causes of Death Collaborators. Global, regional, and national age-sex-specific mortality for 282 causes of death in 195 countries and territories, 1980-2017: a systematic analysis for the global burden of disease study 2017. *Lancet.* 2018;392:1736-88. DOI PubMed PMC
3. Tong Z, Xie Y, Li K, Yuan R, Zhang L. The global burden and risk factors of cardiovascular diseases in adolescent and young adults, 1990-2019. *BMC Public Health.* 2024;24:1017. DOI
4. Daseke MJ 2nd, Tenkorang MAA, Chalise U, Konfrst SR, Lindsey ML. Cardiac fibroblast activation during myocardial infarction wound healing: fibroblast polarization after MI. *Matrix Biol.* 2020;91-92:109-16. DOI PubMed PMC
5. Wolff von Gudenberg R, Iske J, Roeschl T, et al. The Yin and Yang of cellular senescence in ischemia-induced myocardial injury. *Trends Cardiovasc Med.* 2026;36:281-92. DOI PubMed PMC
6. Huang W, Hickson LJ, Eirin A, Kirkland JL, Lerman LO. Cellular senescence: the good, the bad and the unknown. *Nat Rev Nephrol.* 2022;18:611-27. DOI PubMed PMC
7. Demaria M, Ohtani N, Youssef SA, et al. An essential role for senescent cells in optimal wound healing through secretion of PDGF-AA. *Dev Cell.* 2014;31:722-33. DOI PubMed PMC
8. Krizhanovsky V, Yon M, Dickins RA, et al. Senescence of activated stellate cells limits liver fibrosis. *Cell.* 2008;134:657-67. DOI PubMed PMC
9. Zhu F, Li Y, Zhang J, et al. Senescent cardiac fibroblast is critical for cardiac fibrosis after myocardial infarction. *PLoS One.* 2013;8:e74535. DOI PubMed PMC
10. Chen R, Dakhili SAT, Gerulskis R, et al. Cysteine oxidation of a redox hub within complex I can facilitate electron transport chain supercomplex formation. *J Biol Chem.* 2025;301:110555. DOI PubMed PMC
11. McAuley JR, Freeman TJ, Ekambaram P, Lucas PC, McAllister-Lucas LM. CARMA3 is a critical mediator of G protein-coupled receptor and receptor tyrosine kinase-driven solid tumor pathogenesis. *Front Immunol.* 2018;9:1887. DOI PubMed PMC
12. Cheng L, Wei Z, Yang Z, et al. Carma3 protects from liver injury by preserving mitochondrial integrity in liver sinusoidal endothelial cells. *J Immunol.* 2022;209:456-64. DOI
13. Shi D, Zhang Z, Kong C. CARMA3 transcriptional regulation of STMN1 by NF-κB promotes renal cell carcinoma proliferation and invasion. *Technol Cancer Res Treat.* 2021;20:15330338211027915. DOI PubMed PMC
14. Wu Y, Qi Y, Qiu Z, Chen W. Deficiency of CARMA3 attenuates the development of bleomycin induced pulmonary fibrosis. *Biochem Biophys Res Commun.* 2021;581:81-8. DOI
15. Yao Y, Cao Y, Xu Y, et al. CARMA3 deficiency aggravates angiotensin ii-induced abdominal aortic aneurysm development interacting between endoplasmic reticulum and mitochondria. *Can J Cardiol.* 2023;39:1449-62. DOI
16. Pan M, Xu Y, Wang Y, et al. The therapeutic efficacy comparison of MSCs derived different tissues unveilings anti-apoptosis more crucial than angiogenesis in treating acute myocardial infarction. *Stem Cell Res Ther.* 2025;16:236. DOI PubMed PMC
17. Feng J, Xing M, Qian W, Qiu J, Liu X. An injectable hydrogel combining medicine and matrix with anti-inflammatory and pro-angiogenic properties for potential treatment of myocardial infarction. *Regen Biomater.* 2023;10:rbad036. DOI PubMed PMC
18. Rinderknecht H, Mayer A, Histing T, Ehnert S, Nüssler A. Herbal extracts of ginseng and maqui berry show only minimal effects on an in vitro model of early fracture repair of smokers. *Foods.* 2023;12:2960. DOI PubMed PMC
19. Wang B, Han J, Elisseeff JH, Demaria M. The senescence-associated secretory phenotype and its physiological and pathological implications. *Nat Rev Mol Cell Biol.* 2024;25:958-78. DOI

20. Chen H, Zhan Z, Lu M, et al. FOXP1 deficiency exacerbates cellular senescence in $PM_{2.5}$-induced renal injury. *Ecotoxicol Environ Saf.* 2026;314:120071. DOI
21. Barros-Gomes S, Roger VL, Pislaru SV, Kimura T, Pislaru C, Enriquez-Sarano M. Cardiac remodeling in acute myocardial infarction: prospective insights from multimodality ultrasound imaging. *Echocardiography.* 2021;38:2032-42. DOI PubMed PMC
22. Frangogiannis NG. Cardiac fibrosis. *Cardiovasc Res.* 2021;117:1450-88. DOI PubMed PMC
23. Hu G, Chen W, Zhou X, et al. Aerobic exercise stabilizes atherosclerotic plaques by suppressing miR-15a-5p-mediated repression of semaphorin-3A in vascular smooth muscle cells. *Life Sci.* 2026;389:124226. DOI
24. Fernández-Yagüe MA, Barber GF, Del Campo A, et al. FAK modulates immune response and fibroblast activation in biomaterial-induced fibrosis. *Biomaterials.* 2026;330:124010. DOI PubMed PMC
25. Frantz S, Hundertmark MJ, Schulz-Menger J, Bengel FM, Bauersachs J. Left ventricular remodelling post-myocardial infarction: pathophysiology, imaging, and novel therapies. *Eur Heart J.* 2022;43:2549-61. DOI PubMed PMC
26. Akins KA, Arkatkar A, Flinn MA, et al. Runx1 in postn-expressing fibroblasts but not cardiomyocytes exacerbates adverse cardiac remodeling post-myocardial infarction. *JACC Basic Transl Sci.* 2026;11:101455. DOI PubMed PMC
27. Polten F, Sandu MA, Faix J, et al. Extracellular BRICK1 drives heart repair after myocardial infarction in mice. *Sci Transl Med.* 2026;18:eadx2876. DOI
28. Wei X, Mao Y, Chen Z, Kang L, Xu B, Wang K. Exercise-induced myocardial hypertrophy preconditioning promotes fibroblast senescence and improves myocardial fibrosis through Nrf2 signaling pathway. *Cell Cycle.* 2023;22:1529-43. DOI PubMed PMC
29. Wlaschek M, Maity P, Makrantonaki E, Scharffetter-Kochanek K. Connective tissue and fibroblast senescence in skin aging. *J Invest Dermatol.* 2021;141:985-92. DOI PubMed
30. Spray L, Richardson G, Booth LK, et al. How to measure and model cardiovascular aging. *Cardiovasc Res.* 2025;121:1489-508. DOI PubMed PMC
31. Zhang L, Pitcher LE, Yousefzadeh MJ, Niedernhofer LJ, Robbins PD, Zhu Y. Cellular senescence: a key therapeutic target in aging and diseases. *J Clin Invest.* 2022:132. DOI PubMed PMC
32. Ogrodnik M, Acosta JC, Adams PD, et al. Guidelines for minimal information on cellular senescence experimentation in vivo. *Cell.* 2024;187:4150-75. DOI
33. Bhardwaj S, Gautam RK, Kushwaha S. From senescence to scarring: exploring TGF-β signaling in cellular aging, fibrotic remodeling, and pulmonary fibrosis. *Cytokine Growth Factor Rev.* 2025;86:29-39. DOI PubMed
34. Watson LA, Adelsheim Z, Carter MJ, et al. Persistent and transient senescent cells contribute to brain-barrier development. *Cell.* 2026;189:4295-4309.e6. DOI PubMed PMC
35. Martini H, Passos JF. Cellular senescence: all roads lead to mitochondria. *FEBS J.* 2023;290:1186-202. DOI PubMed PMC
36. Ni H, Hu X, Yang N, et al. Roundup® induces premature senescence of mouse granulosa cells via mitochondrial ROS-triggered NLRP3 inflammasome activation. *Toxicol Res.* 2024;40:377-87. DOI PubMed PMC
37. Benkafadar N, François F, Affortit C, et al. ROS-induced activation of DNA damage responses drives senescence-like state in postmitotic cochlear cells: implication for hearing preservation. *Mol Neurobiol.* 2019;56:5950-69. DOI PubMed PMC
38. Camacho-Encina M, Booth LK, Redgrave RE, Folaranmi O, Spyridopoulos I, Richardson GD. Cellular senescence, mitochondrial dysfunction, and their link to cardiovascular disease. *Cells.* 2024;13:353. DOI PubMed PMC
39. Martinez CS, Zheng A, Xiao Q. Mitochondrial reactive oxygen species dysregulation in heart failure with preserved ejection fraction: a fraction of the whole. *Antioxidants.* 2024;13:1330. DOI PubMed PMC
40. Liu CM, Ma JQ, Sun YZ. Puerarin protects rat kidney from lead-induced apoptosis by modulating the PI3K/Akt/eNOS pathway. *Toxicol Appl Pharmacol.* 2012;258:330-42. DOI PubMed
41. Mercurio L, Bailey J, Glick AB, et al. RAS-activated PI3K/AKT signaling sustains cellular senescence via P53/P21 axis in experimental models of psoriasis. *J Dermatol Sci.* 2024;115:21-32. DOI
42. Zhu H, Chan KT, Huang X, et al. Cystathionine-β-synthase is essential for AKT-induced senescence and suppresses the development of gastric cancers with PI3K/AKT activation. *Elife.* 2022;11:e71929. DOI
43. Zeng XX, Gao DD, Zhang F. Cortex mori radicis[*Morus Alba L. (Moraceae)*] extract alleviates senescence via PI3K/Akt signaling in COPD fibroblasts. *Phytomedicine.* 2024;135:156004. DOI PubMed
44. Tang Q, Markby GR, MacNair AJ, et al. TGF-β-induced PI3K/AKT/mTOR pathway controls myofibroblast differentiation and secretory phenotype of valvular interstitial cells through the modulation of cellular senescence in a naturally occurring in vitro canine model of myxomatous mitral valve disease. *Cell Prolif.* 2023;56:e13435. DOI
45. Zhang P, Zhang N, Hu Y, et al. Role of PI3K/AKT/MAOA in glucocorticoid-induced oxidative stress and associated premature senescence of the trabecular meshwork. *Aging Cell.* 2025;24:e14452. DOI